

# Acoustic Visualization of Cold Flakes and Crack Propagation in Aluminum Alloy Die-Cast Plate

A.K. M. Aziz Ahamed\*, Hiroshi Kato\*\*, Kensuke Kageyama\*\*and Toru Komazaki\*\*\*

\* Graduate School of Science and Engineering, Saitama University, 255, Shimo-Okubu, Sakura-Ku, Saitama, 338-8570, Japan

\*\* Department of Mechanical Engineering, Faculty of Engineering, Saitama University, 255, Shimo-Okubo, Sakura-Ku, Saitama, 338-8570, Japan

\*\*\* Ryobi Limited, Die Casting Division, 762, Mesaki-Cho, Fuchu, Hiroshima 726-0033, Japan

Corresponding author:

A. K.M. Aziz Ahamed  
Graduate School of Science and Engineering  
Saitama University  
255, Shimo-Okubu, Sakura-Ku  
Saitama, 338-8570  
Japan

e-mail: [aziz@mehp.mech.saitama-u.ac.jp](mailto:aziz@mehp.mech.saitama-u.ac.jp)

Tel: +81 48 858 3448 Fax: +81 48 856 2577

## Abstract

Acoustic images received from different depths of aluminum alloy (ADC12) die-cast plates containing coarse cold flakes were compared with microstructures at the same depth. The bright and dark regions in the acoustic images coincided with the oxide layer on the initially solidified surface of the cold flake and the body of the cold flake, respectively. These results show the ability of nondestructive detection of cold flakes by the ultrasonic microscopy. The specimens were then fabricated to contain the cold flake at a center, and tested under three point bend configuration. When the coarse cold flake existed apart from the tensile side surface of the specimen, a crack initiated at a small cold flake on the side surface and propagated in the specimen. In this case the bending strength was almost the same as the tensile strength (285 MPa) of the die-cast plate. When the cold flake existed on the tensile side surface or at a position less than 0.5 mm inside the surface, the crack propagated along the oxide layer of the cold flake. In this case, the bending strength decreased from the tensile strength when the cold flake approached the side surface. A relation between the bending strength and the position of the cold flake in the specimen was discussed from the standpoint of the fracture mechanics and  $K_{Ic}$ , the critical stress intensity factor for this alloy, was found to be 3 to 9 MPa·m<sup>1/2</sup>.

**Keywords:** Acoustic microscopy, Cold flake, Aluminum alloy, Die-castings, Bending strength, Critical stress intensity factor

## 1. INTRODUCTION

Following increasing application for aluminum alloy die-cast products, many studies have been carried out on their mechanical properties, and it has been reported that the mechanical properties were largely influenced by casting defects, such as irregular structures [1 ~ 5] porosities [6] and so on. It has been mentioned that the tensile strength [7] and the fatigue strength [8, 9] of die-casts decreased with the increase in the amount of porosities. However, the irregularities in structure also affect their mechanical properties. Among irregular structures, cold flakes largely reduce the mechanical properties of the die-castings [10, 11] because they contain the oxide layer of poor cohesive bonding with the surrounding matrix. And these oxide layers are often contaminated by lubricant and stuck by fine porosities [12, 13]. To assure reliability of die-cast products, it is vital to detect irregular structures, especially the cold flake, for which the nondestructive evaluation plays a very important role. The authors [14] carried out the ultrasonic measurement for aluminum alloy (ADC12) die-cast plates containing cold flakes and showed that the cold flake can be detected nondestructively. Moreover to improve the reliability of die-cast products, it is necessary to specify size and position of the cold flake.

In the present work, the acoustic microscopy was carried out with aluminum alloy die-cast plates (ADC12) containing cold flakes to examine detectability of cold flakes. Furthermore, it was postulated if a position of the cold flake is known, the cold flake can be arranged at a required position with a required orientation in the specimen to examine the influence of the position and the orientation of the cold flake on the mechanical properties of die-cast plates.

Concerning the influence of inclusions on the mechanical properties of

materials, researches have been carried out from the standpoint of the fracture mechanics. Murakami et al. [15 ~ 17] examined the effect of nonmetallic inclusions on the fatigue strength of the high strength steel, and showed that the area, the position and the shape of the inclusion influenced the threshold stress intensity factor range  $\Delta K_{th}$  and the fatigue limit in high strength steels. Mayer et al. [18] examined the effect of porosities (voids and shrinkage) on the fatigue property of die-cast magnesium and aluminum alloys and showed if the porosity was equivalent to an initial crack, the fatigue limit was correlated to the critical stress intensity amplitude ( $\Delta K_{cr}$ ). Skallereud et al. [19] examined effects of shrinkage cavities and gas pores on fatigue properties of aluminum alloys, and showed shrinkage cavities significantly reduced the lifetime of the cylindrical aluminum specimen, and if the pore diameter was larger than 0.2 mm, a typical fatigue crack initiated around pores on or near the specimen surface.

Initiative has also been taken to show the importance of cold flake size and position to control the mechanical properties. Therefore, specimens were fabricated to contain the cold flake at different location, and subjected to a three-point bending test under acoustic microscopy to observe initiation and propagation of a crack in the specimen. Then a relation between the bending strength and the position of the cold flake was discussed from the standpoint of the fracture mechanics.

## **2. EXPERIMENTAL PROCEDURE**

### **2.1 Preparation of Materials**

In the present study, aluminum alloy (ADC12, a nominal composition of Al – 11 mass% Si – 2.5 mass% Cu) die-cast plates of two different geometries (plates-A: 6.8 mm thickness, 174 mm length and 50 mm width, and plates-B: 4.0 mm thickness, 300

mm length and 100 mm width) were used. The plate-A was used in the experiment for detection of cold flakes after separating it into three-square plates as shown in **Fig. 1**. The plate-B was used in the bending test after detection of cold flakes in the required position. The casting procedure was carried out with wider gates after longer shot time lags to contain greater cold flakes of some millimeter in size.

## **2.2 Acoustic Microscopy and Ultrasonic Measurement**

The acoustic microscopy was carried out with the scanning acoustic microscope (SAM, by Hitachi Kenki Co. Ltd) by using a probe generating a longitudinal wave of 50 MHz in frequency and focal distance of 12 mm in water.

For detection of cold flakes, acoustic images were taken at positions 0.5 mm to 2 mm below the surface of the plate-A at an interval of 0.1 mm in an area of 9.9 mm × 9.9 mm with a pitch of 16.5 μm. Consecutive images were taken and then combined to obtain an image of 40 mm × 40 mm covering almost the cross section of the specimen. Before bending test of the plate-B, acoustic images were taken at positions 0.5 mm to 2 mm below the surface at an interval of 0.5 mm in an area of 9.9 mm × 9.9 mm with a pitch of 16.5 μm, and combined to obtain an image of 140 mm × 90 mm covering almost the cross section of the specimen. The acoustic images were also taken from the reverse surface of the plate-B to obtain images at positions 0.5 mm to 3.5 mm below the obverse surface.

For comparison, the ultrasonic measurement was also carried out on some specimens with the immersion method. In the measurement, a probe generating a longitudinal wave of 20 MHz in frequency and of a focal distance of 25.4 mm in water was used, and the ultrasonic wave was focused at a half thickness of the specimen.

### 2.3 Observation of microstructures

After acoustic microscopy, the plates-A were sectioned, polished and etched at positions 0.5 mm to 2 mm below the surface at an interval of 0.1 mm. The etching was carried out by using a water solution of 2 mass% NaOH. An optical microscope was also used to observe cold flakes.

### 2.4 Bending Test

After detection of cold flakes in the plate-B by SAM, rectangular pieces were cut off from the plate to contain a cold flake at the center, as shown in **Fig. 2**. In the figure, bright regions like a nebula are from coarse cold flakes. Then specimens for the bending test were fabricated as shown in **Fig. 3**, and the three-point bending test was carried out under SAM by gradually screwing a bolt at a center of the specimen, as shown in **Fig. 4**.

A bending strength was estimated from a deflection of the specimen at fracture with a following procedure. First, a relation between an axial strain on a tension side surface (TSS) and the deflection of the specimen was obtained with a strain gauge mounted at the center of the specimen. Then a stress-strain relation of the alloy die-cast plate was obtained by the tensile test, and finally a relation between the bending stress on TSS and the deflection was obtained.

After bending test, the fracture surface was observed through scanning electron microscope (SEM) at an accelerating voltage of 25 KV and a sample current of 90 ~ 120  $\mu$ A to examine the crack propagation path.

### 3. RESULTS AND DISCUSSION

#### 3.1 Relation between acoustic images and microstructures

Typical acoustic images obtained at different depths are shown in **Fig. 5**. In these images, there are different regions of brightness, such as a bright region, a gray region and a dark region. In the gray region, dispersing small bright spots are the reflections from silicon crystals in the eutectic structure. **Figure 6** compares an acoustic image taken at 1.6 mm below the surface of the specimen with microstructures at the same depth. A dark region (A Fig. 6(a)) is in good agreement with a body of the cold flake (Fig. 6(b)). A bright region (B in Fig. 6(a)) is also in good agreement with the oxide (Fig. 6(c)).

For further clarification, the acoustic image was compared with the intensity distribution obtained by the ultrasonic measurement. **Figure 7** compares bright and dark regions in the acoustic image with intensity distributions in the thickness direction. The dark region (A in Fig. 7(a)) was in good agreement with a low intensity backscattered wave appearing from 1.5 mm to 2.7 mm below the surface (Fig. 7(b)). The bright region (B in Fig. 7(a)) observed in the acoustic image 1.6 mm below the surface was in good agreement with a reflection echo (Fig. 7(c)) from the oxide layer. Since the body of the cold flake contains smaller microstructures than the matrix, they have a smaller attenuation coefficient [20] to cause a lower intensity of the backscattered wave. Therefore the body of the cold flake appears as the dark region in the acoustic image. Inclusions of the second phase reflect the ultrasonic wave because of different acoustic impedance resulting in bright regions.

From these results, it was found that the cold flake was visualized in the acoustic image: The oxide layer was represented as the bright region, and the body of the cold

flake was represented as the dark region, as shown schematically in **Fig. 8**. Since cold flakes (>1 mm) are greater than the silicon particle, they can be distinguished in acoustic images.

### **3.2 Relation between crack propagation path and position of cold flake**

The three-point bending test was carried out with specimens containing the cold flake. In **Fig. 9**, acoustic images of a specimen containing the cold flake about 4 mm inside the side surface are shown at different deflections. In these figures, the load was applied on the upper side surface at the center of the specimen as indicated by arrows in the figure, and the maximum tensile stress appeared at the center of the lower side surface (tension side surface, TSS). A crack initiated on TSS and propagated in the specimen apart from the cold flake inside the surface (hereafter referred to as the inside cold flake). As shown in **Fig. 10**, a small cold flake appearing on TSS was observed in the fracture surface. Other observations of the specimens containing the cold flake few millimeters inside TSS showed that the crack initiated at a fine cold flake on TSS, and propagated in the specimen independent of the inside coarse cold flake.

Then the crack propagation was observed in the specimens containing the cold flake on TSS. In this case, the specimen broke at a very small deflection, and the crack propagated through a boundary between the oxide layer of the inside cold flake and the matrix as shown in **Fig. 11**. **Figure 12** shows the SEM micrograph on the fracture surface. From these results, it was assumed that when the cold flake existed just inside TSS, the crack might initiate and propagate along the oxide layer. **Figure 13** shows a crack propagation in the specimen with the cold flake existing 0.1 mm inside TSS, and the crack propagated through the oxide layer as shown in **Fig. 14**. However, it was not

clarified whether the crack initiation site was at the tip of the oxide layer, or not.

**Figure 15** shows the relation between a bending strength and a position of the cold flake. In the figure, a horizontal dashed line indicates the tensile strength (285 MPa) of the aluminum alloy (ADC12) die-cast plate free from the coarse cold flake. When the oxide layer of the cold flake was arranged parallel to the specimen axis, the bending strength was independent of the position of the cold flake but was the same as the tensile strength. When the oxide layer was perpendicular to the specimen axis, the bending strength was dependent on the position of the cold flake: when the cold flake existed at a position 0.5 mm or greater inside TSS, the bending strength took almost a constant value being equal to the tensile strength, and the crack initiated and propagated independently of the inside cold flake. When the cold flake existed less than 0.5 mm inside TSS, the bending strength decreased with reducing depth of the cold flake and the crack propagated through the oxide layer of the inside cold flake.

### **3.3 Evaluation of fracture toughness**

In the aluminum alloy die-cast, cold flakes are thought to cause crack initiation and propagation [11], because the oxide/matrix bonding strength is weak and the oxide layer can thus be separated easily from the matrix at a lower level of applied stress. In this section, the oxide layer on the cold flake was treated as a defect equivalent to a crack, and the fracture mechanics was applied to obtain a critical stress intensity factor at fracture ( $K_c$ ). In Fig. 15, there are two types of data on the crack propagation: the type I for the crack propagated through the cold flake, and the type II for the crack propagated independent of the selected cold flake. In calculation of the stress intensity factor, only data of the type I were used and it was assumed that the crack initiated at a

tip of the cold flake and propagated along the oxide layer.

For calculation of the stress intensity factor, there are two models depending on a position of the cold flake. One is for an embedded cold flake and the other is for a surface one, as shown in **Fig. 16**. Since the bending test was carried out in the present work, a reverse side to the applying load was in tension. Therefore, for simplicity, a model with embedded cold flake suffered an axial tension was used for calculation of the stress intensity factor in consideration of a linear change of the stress in the thickness direction in the bending test. Ishida and Noguchi [21] developed formulae of the stress intensity factors  $K_{I,A}$  for an embedded elliptical crack in the finite thickness plate under tension, in which the crack was located at an arbitrary position close to one of the plate surfaces and with one of its principal diameters parallel to the plate surfaces. In the present study, the shape of the cold flake was approximated to an ellipse, and the critical stress intensity factor  $K_c$  was obtained for the embedded cold flake as shown in **Fig. 17**. In the figure, the fracture toughness of  $11 \sim 14 \text{ MPa} \cdot \text{m}^{1/2}$  [23] was indicated as a hatched zone. In calculation, at first, the principal diameter of the embedded cold flake was obtained from the acoustic image. Since the acoustic image was obtained at an interval of 0.5 mm, the size of the cold flake was underestimated, and the critical stress intensity factor  $K_c$  (solid circles in Fig. 17) took higher values than the fracture toughness. Then, the position and the principal diameter for the cold flake were precisely measured on the fracture surface, and  $K_c$  was obtained as indicated by rectangles in Fig. 17. The value of  $K_c$  approached to the fracture toughness of the bulk. However, two of  $K_c$  in the figure were still greater than others. This may be due to the extra large cold flakes ( $3.1 \text{ mm}^2$  and  $2.8 \text{ mm}^2$  in area) with sharp edge as shown in Fig. 14, and these were out of model in calculation.

For the surface cold flakes as shown in Fig. 16(b), the analysis was performed with formulae obtained by Newman and Raju [22, 24] with a model that a surface crack suffers a bending force.  $K_c$  obtained for the surface cold flake is shown as a circle in Fig. 17. Principal diameters of the cold flake were obtained on the fracture surface.  $K_c$  for the surface cold flake ranged from 3 to 9  $\text{MPa} \cdot \text{m}^{1/2}$  and was lower than that of the embedded one and the fracture toughness.

Kanazawa et al. [23] obtained the fracture toughness of the alloy by using CT specimens without a coarse cold flake. However the present work confirmed that a crack started from the surface or near the surface cold flake at lower stresses in the bending test. Therefore the stress intensity factor estimated for the specimen with the surface cold flake was more satisfactory.

#### **4. CONCLUSIONS**

The acoustic microscopy was carried out with aluminum alloy (ADC12) die-cast plates containing coarse cold flakes, and acoustic images were compared with microstructures on the cross section. Then the bending test was carried out with the specimen containing the cold flake at the center under acoustic microscopy. Following conclusions were obtained.

- 1) There were some regions of different brightness in the acoustic image. The bright and dark regions were in good agreement with the cold flakes: the bright region coincided with the oxide layer appearing on the initially solidified surface of the cold flake or the oxide inclusion, and the dark region was coincident with the body of the cold flake. These results confirm ability of nondestructive detection of cold flakes, especially the oxide layer, with the acoustic microscopy.

- 2) When the cold flake existed apart from the side surface, the bending strength took a constant value of 275 ~ 290 MPa being equal to the tensile strength of 285 MPa. In this case, a crack initiated at a small cold flake on the side surface and propagated in the specimen independent of the inside cold flake. When the cold flake existed on the tension side surface (TSS) or at a depth less than 0.5 mm from TSS, the crack initiated at a lower bending strength than that of the bulk specimen, and propagated through the boundary between the oxide layer and the matrix.
- 3) Assuming that the oxide layer of the cold flake is equivalent to the crack, the critical stress intensity factor at fracture  $K_c$  was evaluated from the bending strength of the specimen with the cold flake on or near TSS.  $K_c$  for the surface cold flake took a value of 3 to 9 MPa·m<sup>1/2</sup>, which was lower than that for the embedded cold flake and the fracture toughness of 11 to 14 MPa·m<sup>1/2</sup> for die-cast aluminum (ADC12) alloy.

## ACKNOWLEDGEMENTS

The authors are very grateful to Dr. M. Nishi, Japan Die Casting Association for his valuable comment. The authors also acknowledge Dr. Y. Arai, Associate professor of Saitama University, for his instruction to operate acoustic microscope. The acoustic images were taken by using the acoustic microscope in Molecular Analysis and Life Science Center, Saitama University.

## REFERENCES

- [1] H. Iwahori, K. Tozawa, Y. Yamamoto and M. Nakamura, *J. Japan Inst. Light Metals* 34 (1984) 389-394. (in Japanese)
- [2] N. Nishi, T Komazaki and Y. Takahashi, *IMONO* 63 (1991) 347-352. (in Japanese)
- [3] T. Komazaki, Y. Maruyama and N. Nishi, *IMONO* 67 (1995) 258-264. (in Japanese)
- [4] W.G. Walkington: *Die Casting Defects*, North American Die Casting Association, Rosemont, Illinois, (1997) 155-158.
- [5] H. Nomura, E. Kato, Y. Maeda and S. Okubo, *J. JFS* 73 (2001) 656-661. (in Japanese)
- [6] M. Okayasu, K. Kanazawa and N. Nishi, *J. JFS* 71 (1999) 301-306. (in Japanese)
- [7] M. Okayasu, K. Kanazawa and N. Nishi, *J. JFS* 70 (1998), 779-785. (in Japanese)
- [8] M. Avalle, G. Belingardi, M.P. Cavatorta and R. Doglione, *Int. J. Fatigue*, 24 (2002) 1-9.
- [9] H. Mayer, M. Papakyriacou, B. Zettl and S.E. Stanzl-Tschegg, *Int. J. Fatigue* 25 (2003) 245-256.
- [10] H. Iwahori, K. Tozawa, T. Asano, T. Yamamoto, M. Nakamura, M. Hasimoto and S. Uenishi, *J. Japan Inst. Light Metals* 34 (1984) 525-530. (in Japanese)
- [11] T. Komazaki, N. Nishi and Y. Takahashi, *IMONO* 65 (1993) 191-196. (in Japanese)
- [12] Y. Sato, I. Ohnaka, J-D Zhu and H. Yasuda, *J. JFS* 74 (2002) 235-239. (in Japanese)

- [13] I. Ohnaka, A. Sugiyama, H. Onda, A. Kimatsuka, H. Yasuda, J-D Zhu and H. Zhao, Proc. Conf. Modeling of Casting and Solidification Processes 2004, ed. by W.S. Hwang, Metal Industrials Research and Development Centre, Tainan, (2004) 3-11.
- [14] H. Kato, T. Suzuki, Y. Annou and K. Kageyama, Mater. Trans. 45 (2004) 2403-2409.
- [15] Y. Murakami and S. Kodama and S. Konuma, J. Japan Soc. of Mech. Eng. (A) 54 (1988) No-500, 688-696. (in Japanese)
- [16] Y. Murakami and H. Usuki, J. Japn Soc. Mech. Eng. (A), 55 (1989), No-510, 213-221. (in Japanese)
- [17] Y. Murakami and Y. Ummura and K. Kawakami, J. Japan Soci. Mech. Eng. (A), 55 (1989), No-509, 58-62. (in Japanese)
- [18] H. Mayer, M. Papakyriacou, B. Zettl and S.E. Stanzl-Tschegg, Int. J. Fatigue, 25(2003) 245-256.
- [19] B. Skallerud, T. Iveland and G. Harkegard, Eng. Frac. Mech., 44 (1993), No. 68, 57-874.
- [20] E. P. Papadakis: J. Acoust. Soc. Am. 37 (1965), 703-710.
- [21] M. Ishida and H. Noguchi, Eng. Frac. Mech. 20 (1984) No. 3, 387-408.
- [22] J.C Newman, Jr. and I.S. Raju, Eng. Frac. Mech. 15(1981), No 1-2, 185-192.
- [23] K. Kanazawa, K. Chijiiwa, H. Kubata and K. Nakamura, Proc. Japan. Die Casting Assoc., JD94-20 (1994) 170-177. (in Japanese)
- [24] Murakami Y. Stress Intensity Factor Handbook, 02 (1987), 723-724, Oxford, Pergamon Press

### List of Figure caption

- Fig. 1 Die-cast plate of aluminum alloy for detection of cold flake.
- Fig. 2 Preparation of pieces for bending test. Bright regions like nebula are from coarse cold flake.
- Fig. 3 Shape and dimensions of specimen for bending test having a cold flake at a center.
- Fig. 4 Device for three-point bending.
- Fig. 5 Typical acoustic images obtained at different depths below the surface.
- Fig. 6 Comparison of acoustic image with microstructure in cross section at 1.6 mm below the surface.
- Fig. 7 Comparison of dark and bright regions in acoustic image at 1.6 mm below the surface with intensity distributions obtained by ultrasonic measurement.
- Fig. 8 Schematic representation of relationship between acoustic image and cold flakes.
- Fig. 9 Acoustic images of specimen having a cold flake 3.6 mm inside lower side surface under different bending.
- Fig. 10 Fracture surface of specimen in Fig. 9 obtained through SEM.
- Fig. 11 Crack propagation in acoustic images of specimen having a cold flake appearing on lower side surface.
- Fig. 12 Fracture surface of specimen in Fig. 11 obtained through SEM.
- Fig. 13 Crack propagation in acoustic images of specimen having a cold flake 0.1 mm inside lower side surface.
- Fig. 14 Fracture surface of specimen in Fig. 13 obtained through SEM.

- Fig. 15 Relation between position of cold flake and bending strength. Type I: Crack propagated through cold flake, Type II : Crack propagated independent of cold flake.
- Fig. 16 Models for calculation of stress intensity factor. (a) Embedded crack, (b) Surface crack
- Fig. 17 Relation between critical stress intensity factor at fracture  $K_c$ , and position of cold flake.

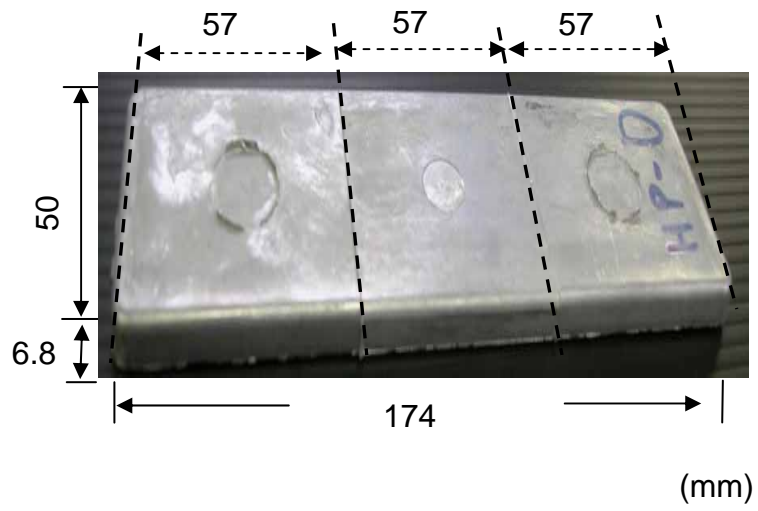


Fig. 1. Die-cast plate of aluminum alloy for detection of cold flake.

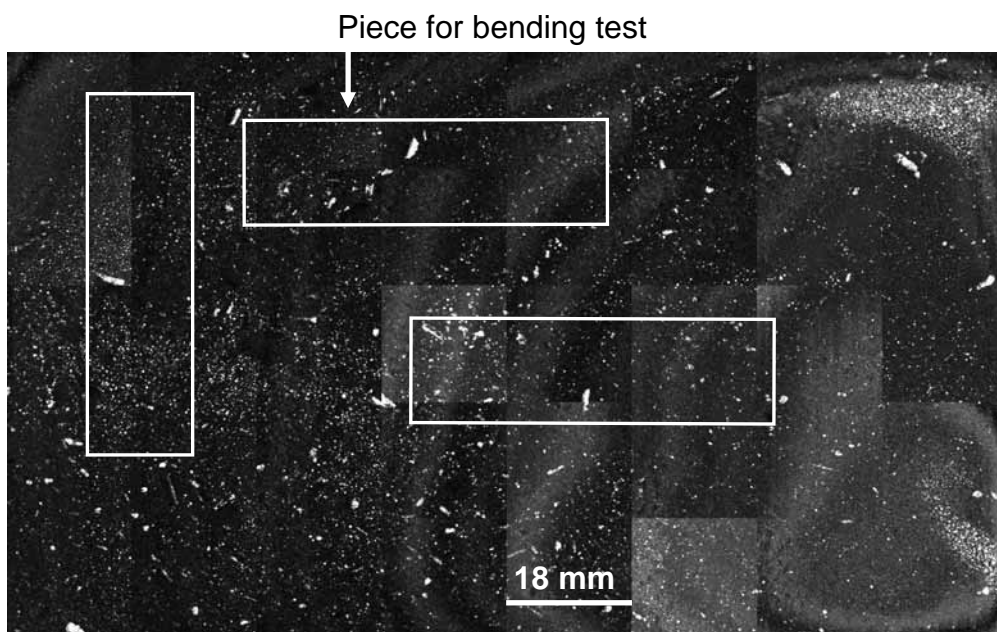


Fig. 2. Preparation of pieces for bending test. Bright regions like a nebula are from coarse cold flakes.

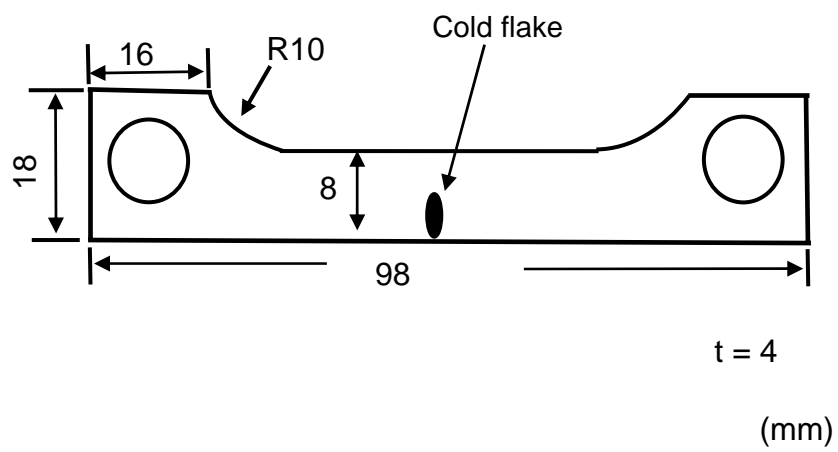


Fig. 3. Shape and dimensions of specimen for bending test having a cold flake at a center.

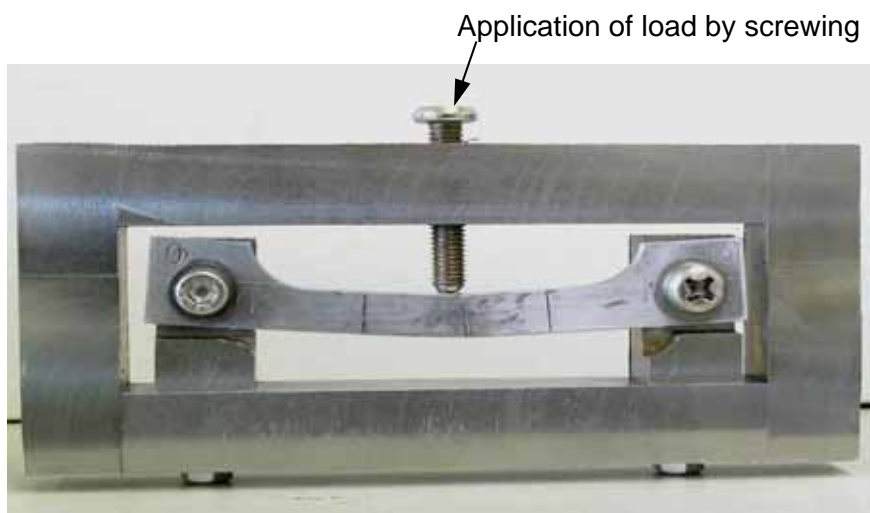


Fig. 4. Device for three point bending.

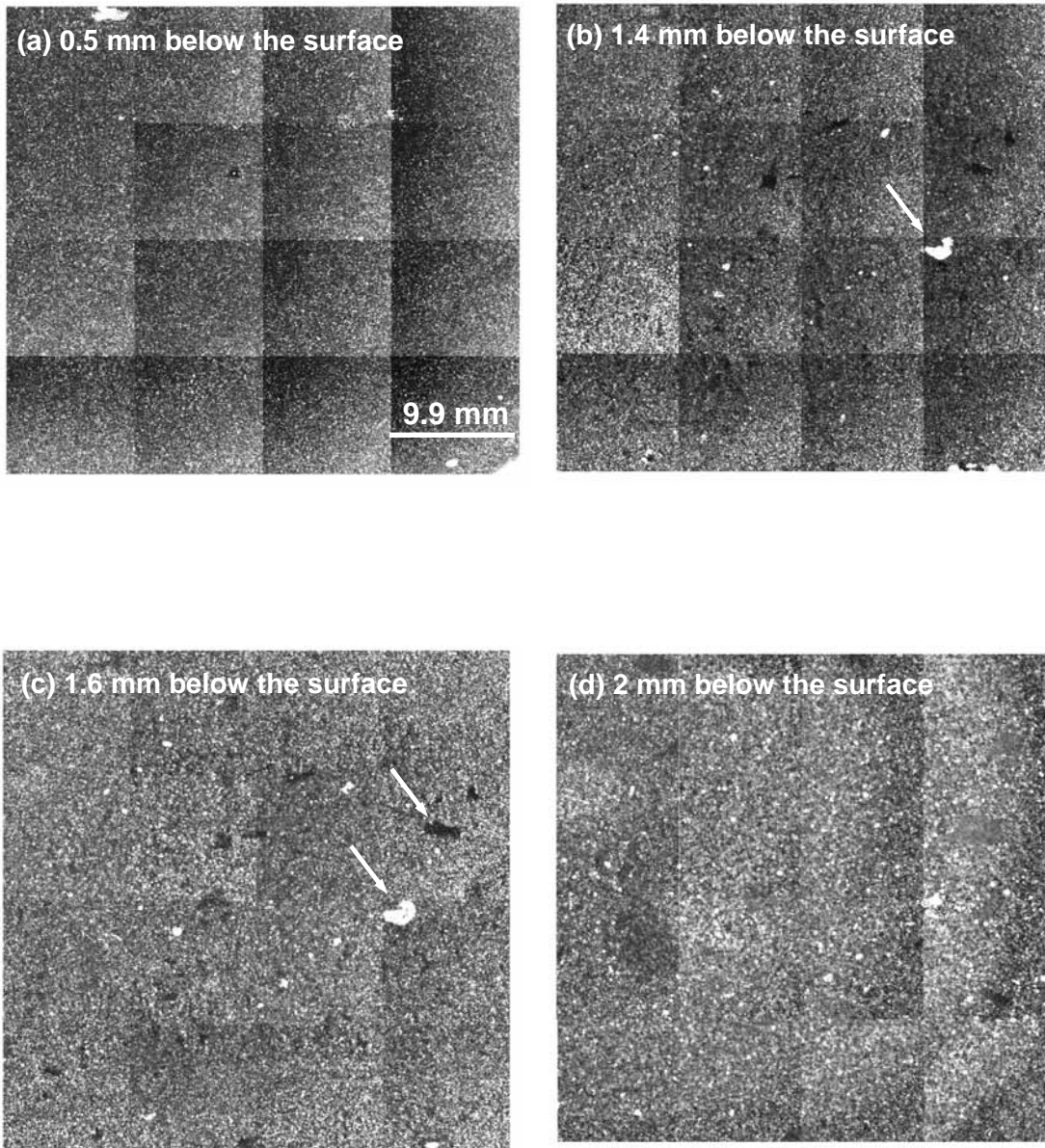
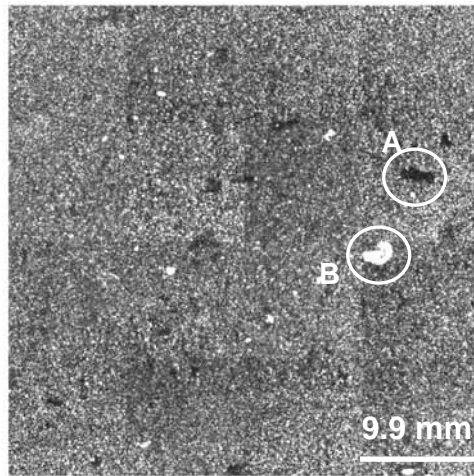
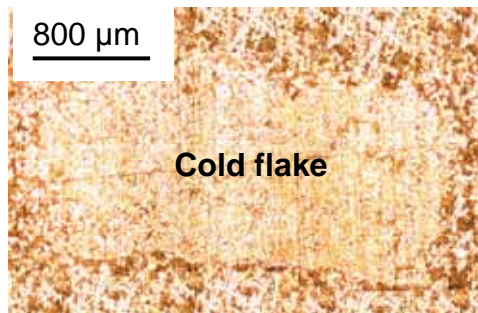


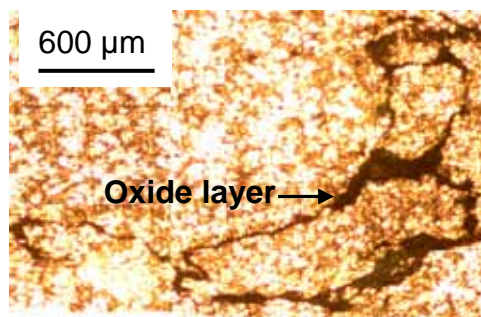
Fig. 5. Typical acoustic images obtained at different depths below the surface.



(a) Acoustic image

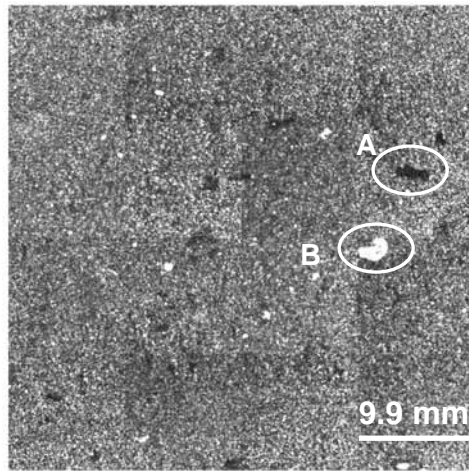


(b) Microstructure at point A

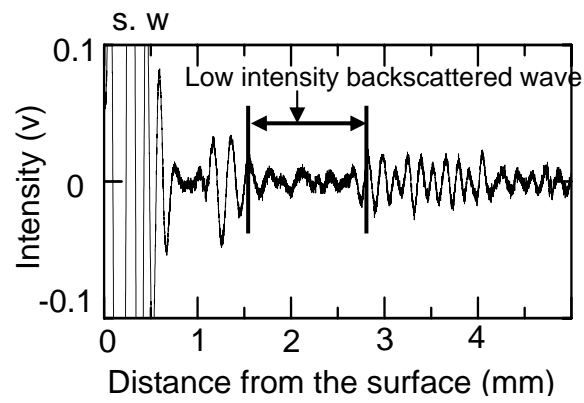


(c) Microstructure at point B

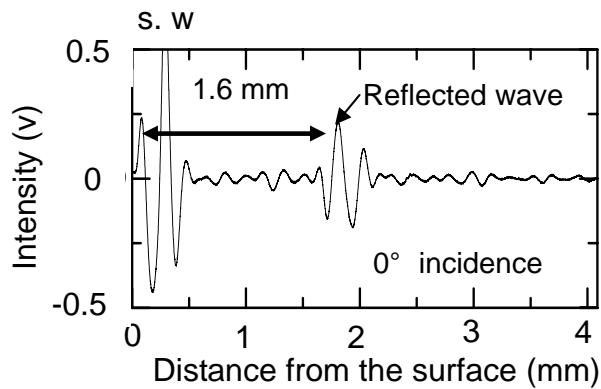
Fig. 6. Comparison of acoustic image with microstructures in cross section at 1.6 mm below the surface.



(a) Acoustic image



(b) At point A



(c) At point B

Fig. 7. Comparison of dark and bright regions in acoustic image at 1.6 mm below the surface with intensity distributions obtained by ultrasonic measurement.

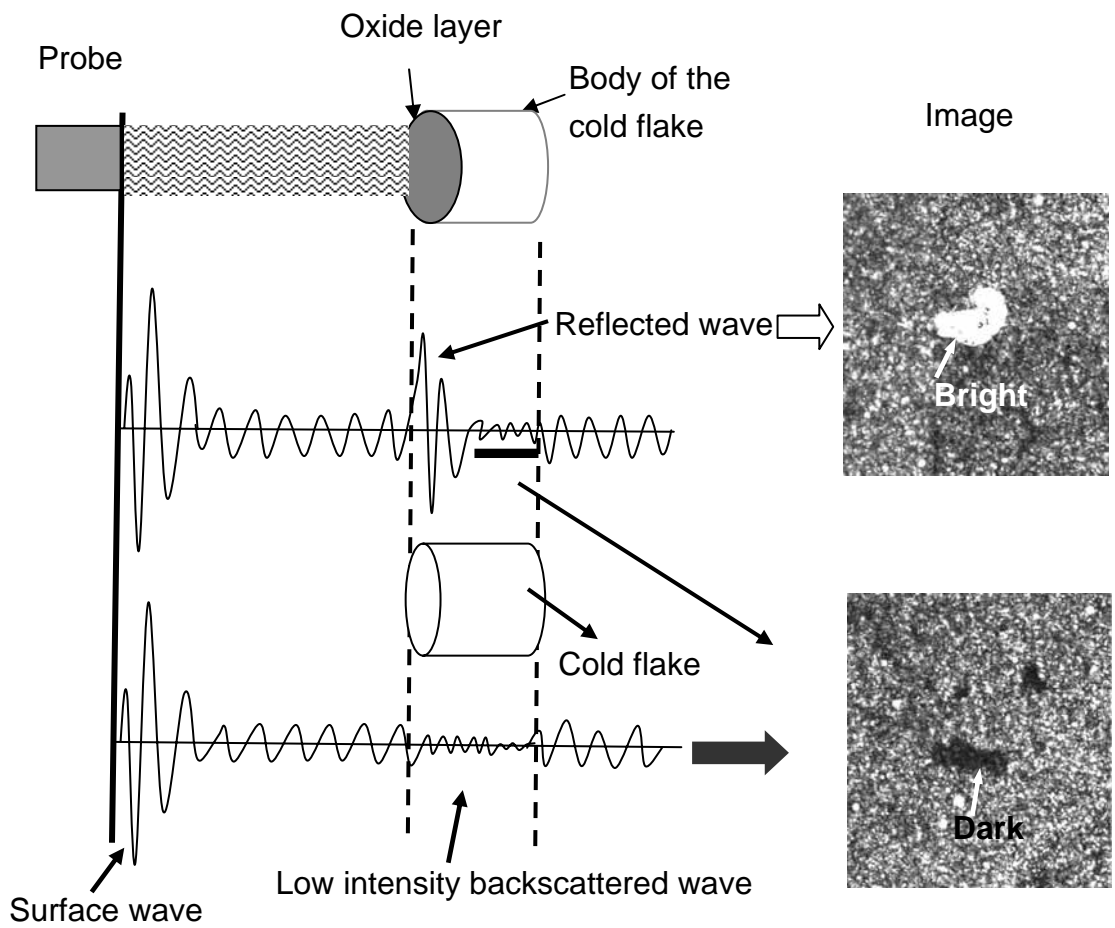


Fig. 8. Schematic representation of relationship between acoustic image and cold flakes.

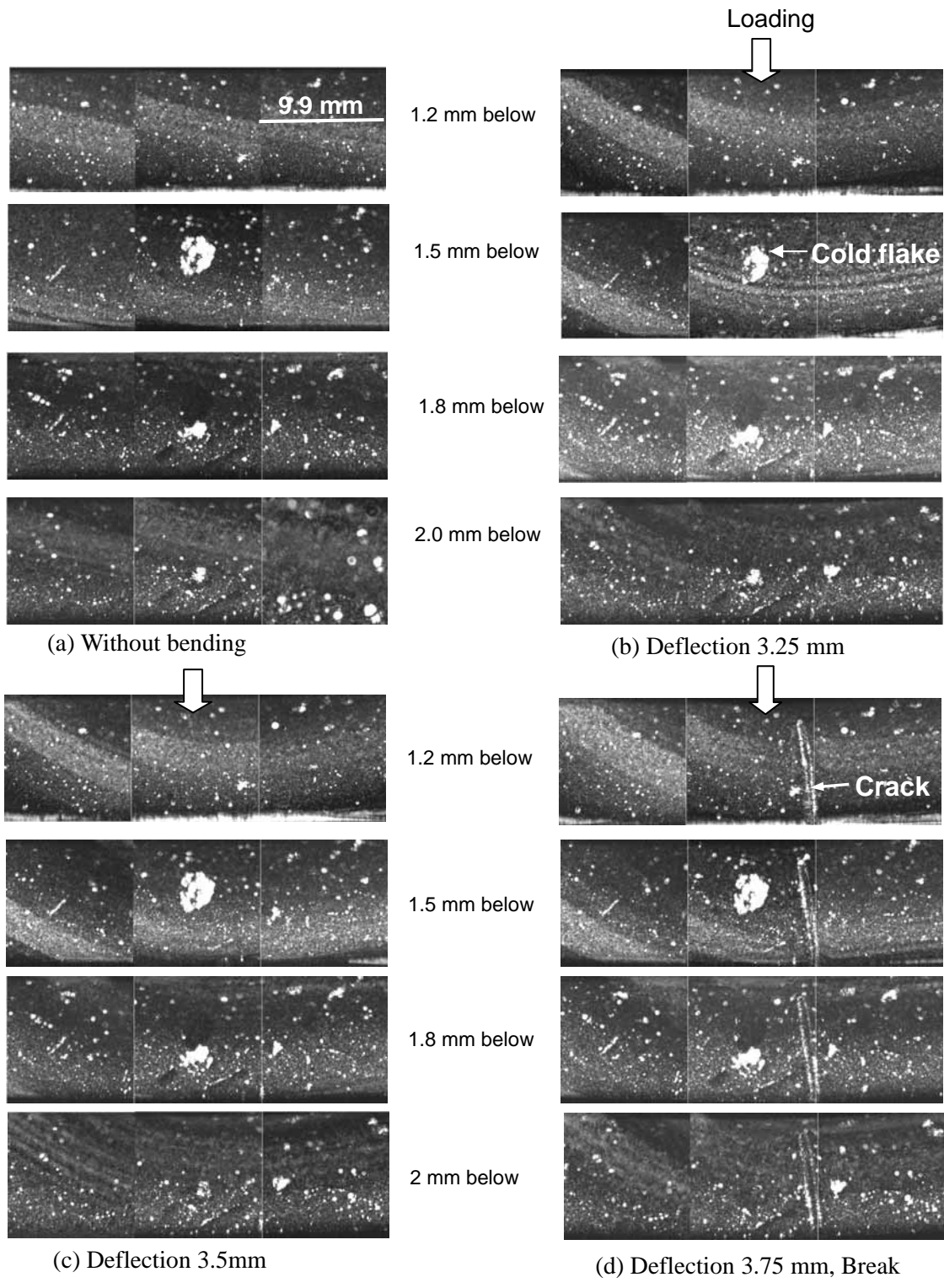
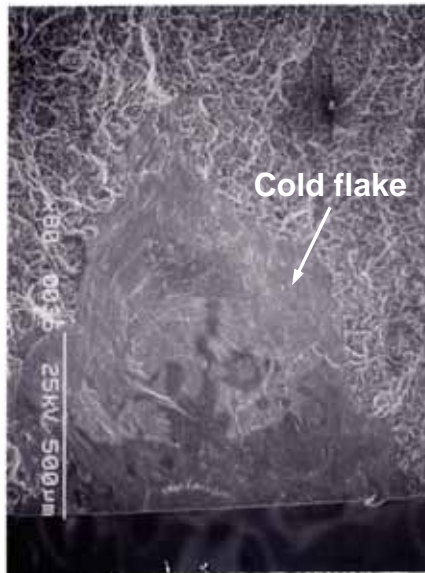


Fig. 9. Acoustic images of specimen having a cold flake 3.6 mm inside lower side surface under different bending.



φ

Fig. 10. Fracture surface of specimen in Fig. 9 obtained through SEM.

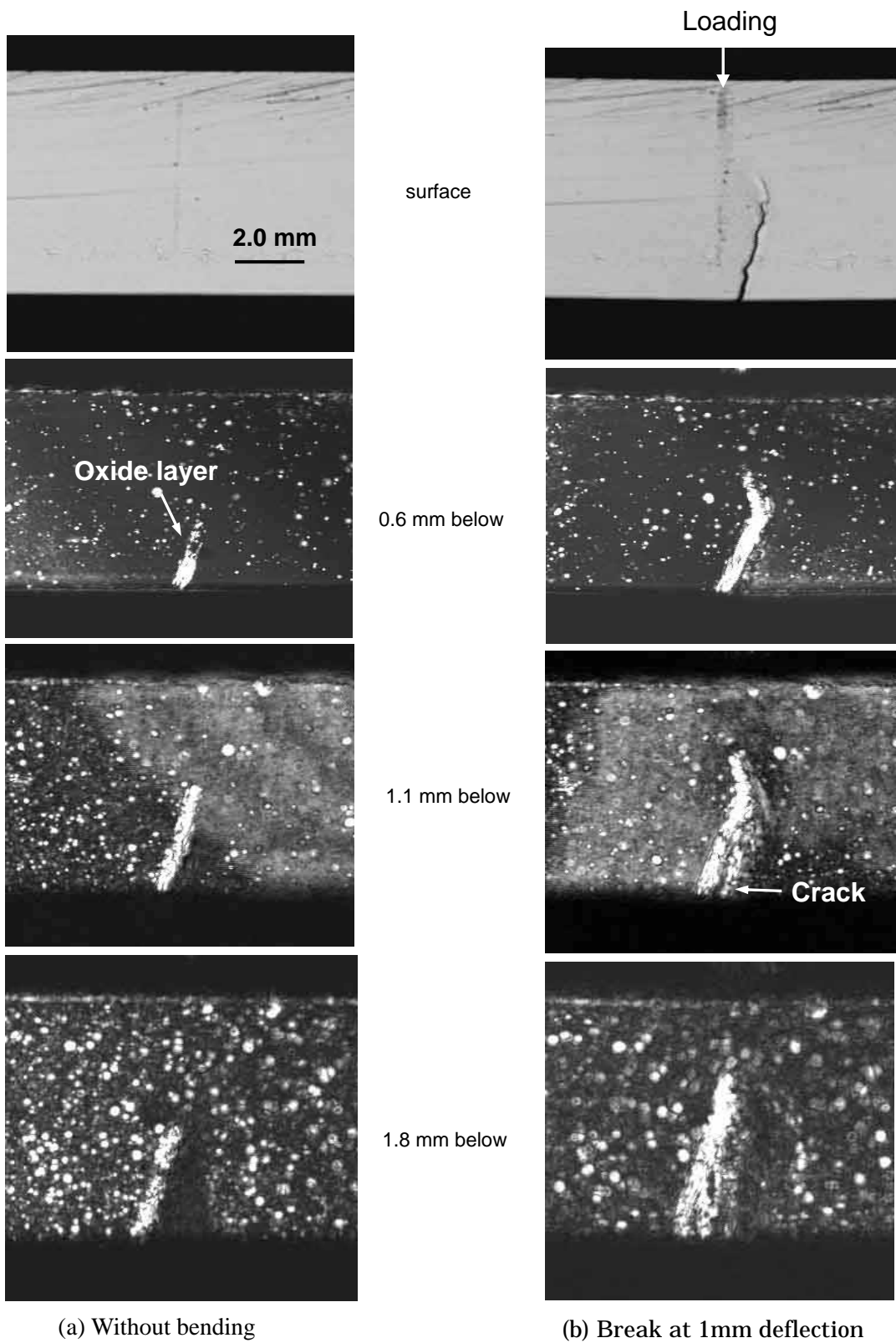


Fig. 11. Crack propagation in acoustic images of specimen having a cold flake appearing on lower side surface.

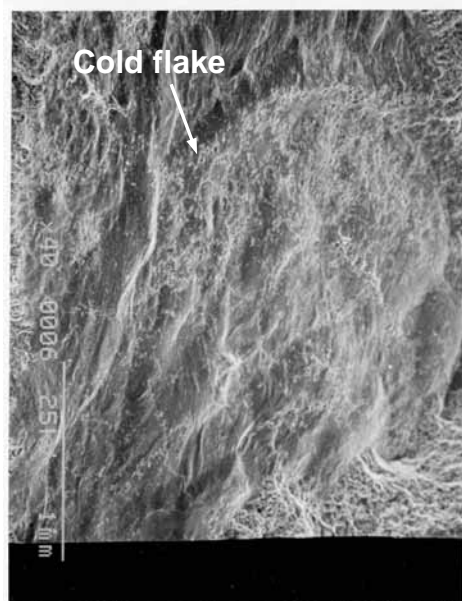


Fig. 12. Fracture surface of specimen in Fig. 11 obtained through SEM.

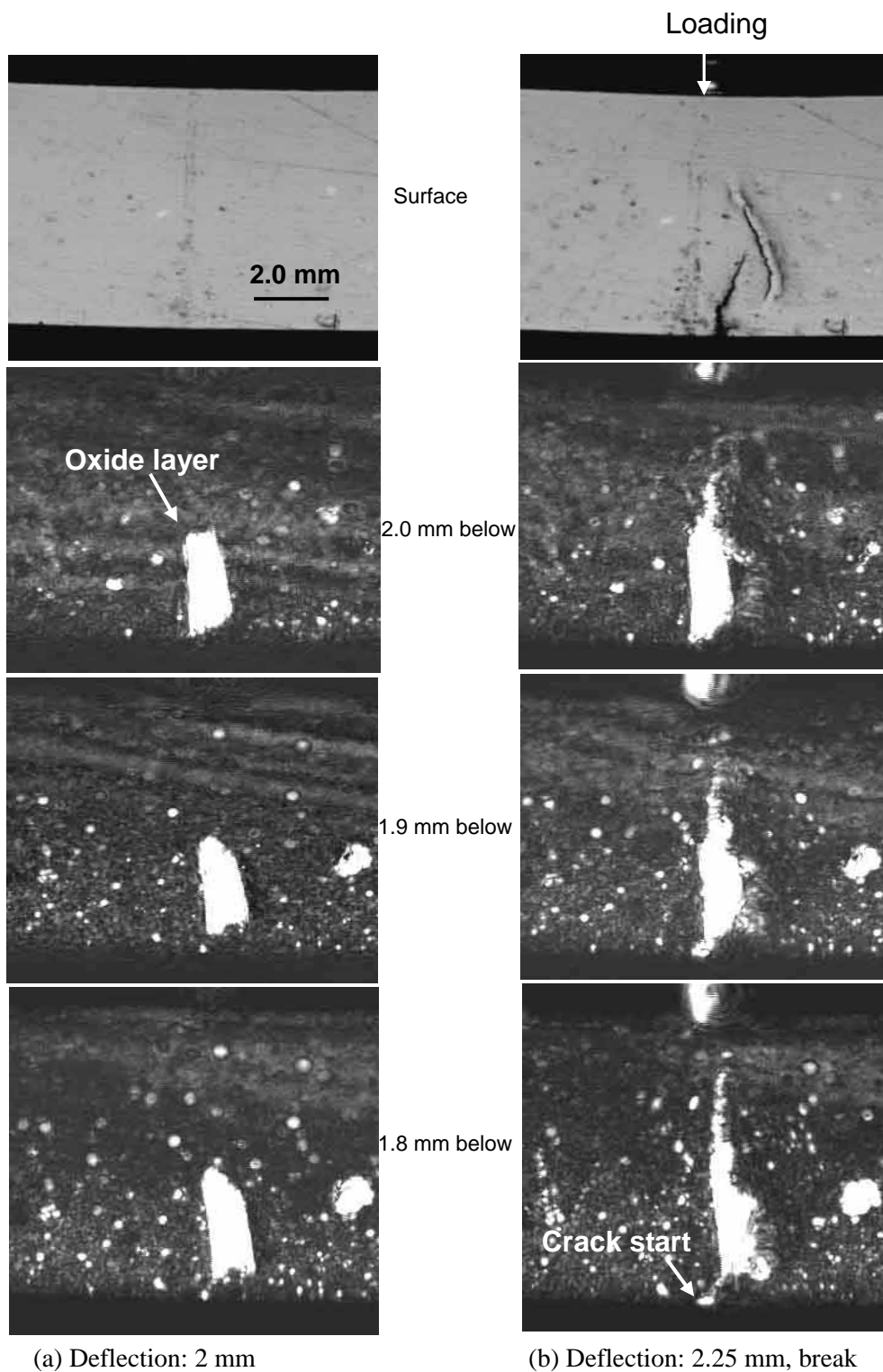


Fig. 13. Crack propagation in acoustic images of specimen having a cold flake 0.1 mm inside side surface.

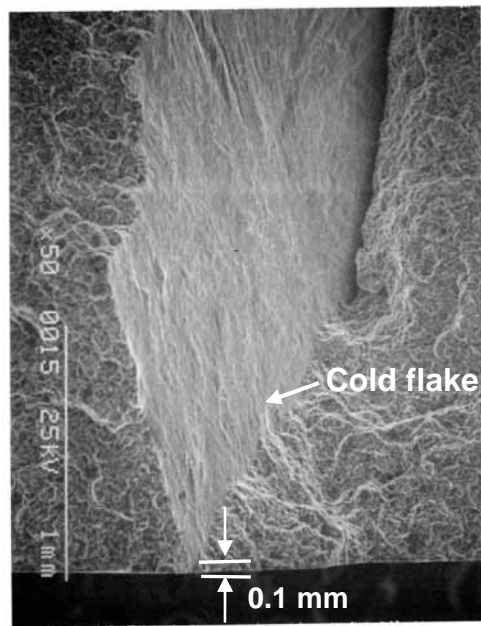


Fig. 14. Fracture surface of specimen in Fig. 13 obtained through SEM.

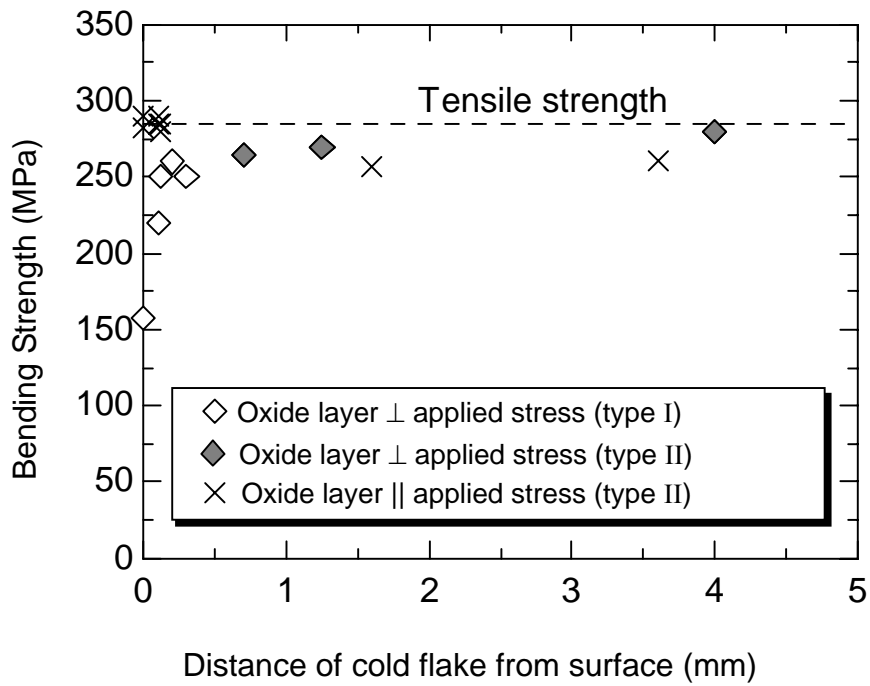
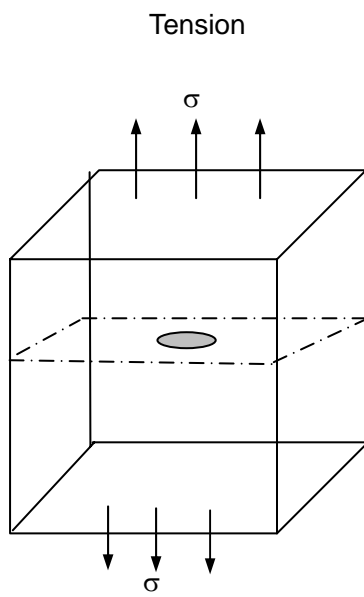


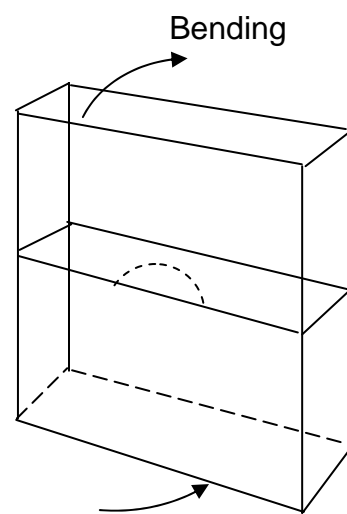
Fig. 15. Relation between position of cold flake and bending strength.

Type I: Crack propagated through cold flake

Type II: Crack propagated independent of cold flake



(a) Embedded cold flake



(b) Surface cold flake

Fig. 16. Models for calculation of stress intensity factor.

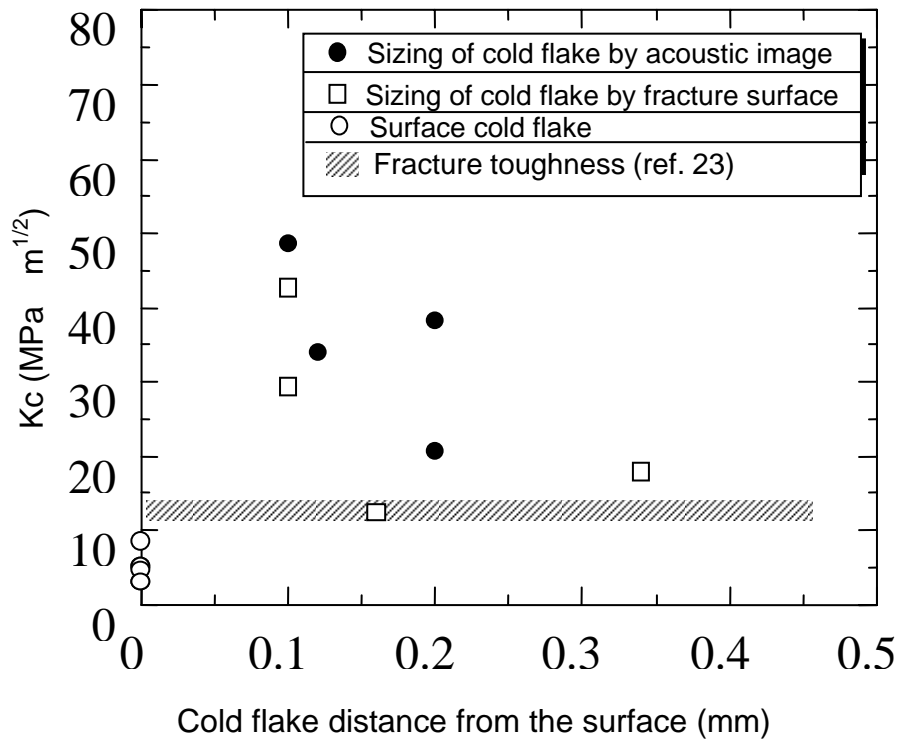


Fig. 17. Relation between critical stress intensity factor at fracture  $K_c$  and position of cold flake.